ISSN 0030-400X, Optics and Spectroscopy, 2015, Vol. 118, No. 3, pp. 364–388. © Pleiades Publishing, Ltd., 2015.

CONDENSED-MATTER SPECTROSCOPY

FT-IR Spectroscopic and DFT Computational Study on Solvent Effects on 8-Hydroxy-2-quinolinecarboxylic Acid[1]

S. Badoğlu and Ş. Yurdakul

Department of Physics, Faculty of Science, Gazi University, Teknikokullar, Ankara 06500, Turkey

e-mail: senayy@gazi.edu.tr

Received June 2, 2014

Abstract—Solvent effects on the spectroscopic, structural, and electronic properties of 8-hydroxy-2-quinolinecarboxylic acid (8HQC) were analyzed theoretically and experimentally. Density functional theory (DFT) B3LYP/6-311++G(d, p) used within polarized continuum model (PCM) to characterize the solvent effects in benzene, diethyl ether, ethanol, and water. Experimental FT-IR spectra in ethanolic and aqueous solutions were recorded and compared with solid phase experimental data. Nucleus independent chemical shifts were calculated as aromaticity indices. Our results show that the spectroscopic, structural, and electronic properties of 8HQC are solvent dependent.

DOI: 10.1134/S0030400X15030066

INTRODUCTION

Theoretical investigations have much applicability in many areas of chemistry such as spectroscopic assignments and characterization of molecular structures [1, 2]. Solvent effects often play an important role in determining conformations, reaction rates, equilibrium constants, and other chemical and biochemical entities [3]. As most chemical reactions occur in the solution phase, the study of solvent effects is very important. These kinds of effects are also considered as pivotal tools for drug design in the pharmaceutical industry because they affect the release, transport and degree of absorption of the drug in the organism, which is important for future development and formulation efforts of the drugs [4].

Currently, a continuum treatment of the solvent through the self-consistent reaction field (SCRF) model is widely employed while studying solvent effects [5]. SCRF continuum models can treat solute's electronic distribution quantitatively. The polarizable continuum model (PCM) by Miertuš, Scrocco, and Tomasi was the first proposed SCRF method [6]. The PCM has proven itself as a reliable tool for describing electrostatic solute-solvent interactions. Employing PCM solvation model within the density functional theory (DFT) is a widely used way for modeling solvent effects [7].

To the best of our knowledge, there are no published data available on solvent effects on the spectroscopic, structural, and electronic properties of 8HQC. In the first part of this paper, we present a theoretical study on the geometrical parameters, vibrational frequencies, and energetics of 8-hydroxy-2-quinolinecarboxylic acid (8HQC) in various solvents. 8HQC contains benzene and pyridine rings besides hydroxyl and carboxylic acid moieties. 8HQC and its derivatives can be used as effective stabilizers against the photo fading of indicator dyes [8, 9]. Also they can be used as the precursor of anti-inflammatory substances [10]. We have used the DFT within the PCM to calculate those properties in four different solvents, and compared the computed data with their counterparts in the gas phase. Nucleus independent chemical shifts (NICS) were calculated as aromaticity indices. The solvents chosen were benzene ($\varepsilon = 2.2706$), ether ($\varepsilon = 4.24$), ethanol ($\varepsilon = 24.852$), and water ($\varepsilon = 78.3553$). In the second part, solution phase experimental FT-IR spectra of the compound were recorded in ethanol and in water, and then compared with the solid phase experimental data. Experimental frequencies were assigned on the basis of the potential energy distributions obtained from DFT-PCM calculations. Theoretical electronic properties were reinvestigated by including solvent both explicitly and implicitly.

EXPERIMENTAL AND COMPUTATIONAL METHODS

8-hydroxy-2-quinolinecarboxylic acid was purchased from Aldrich and used without further purification. FT-IR spectra were recorded between 3500 and 550 cm^{-1} on a Bruker Vertex 80 spectrometer equipped with a Pike MIRacle ATR accessory. For

[1] The article is published in the original.

Table 1. Energies (Hartree) and relative Gibbs energy differences (kcal/mol) of 8HQC in various solvents

	Vacuum [13]	Benzene	Ether	Ethanol	Water
ε	1	2.2706	4.24	24.852	78.3553
E_0	−665.767	−665.773	−665.776	−665.780	−665.781
E	−665.756	−665.762	−665.765	−665.769	−665.770
H	−665.755	−665.761	−665.764	−665.768	−665.769
G	−665.803	−665.809	−665.812	−665.816	−665.817
ΔG(gas-soln)		3.76	8.77	8.30	8.73

E_0: sum of electronic and zero-point energies (E_{elec} + ZPE).
E: sum of electronic and thermal energies ($E_0 + E_{vib} + E_{rot} + E_{transl}$).
H: sum of electronic and thermal enthalpies (E + RT).
G: sum of electronic and thermal free energies (H − TS).

Table 2. Selected geometrical parameters (Å and degrees) of 8HQC

Parameter	Vacuum [13]	Benzene	Ether	Ethanol	Water
2C-16O	1.351	1.353	1.354	1.355	1.355
11C-12C	1.510	1.507	1.506	1.504	1.504
12C-14O	1.203	1.206	1.207	1.210	1.210
12C-15O	1.343	1.342	1.341	1.340	1.339
17H···13N	2.183	2.187	2.191	2.198	2.199
21H···13N	2.060	2.049	2.047	2.048	2.049
17H···13N···21H	78.582	78.025	77.837	77.657	77.633
11C-10C-18H	118.783	119.105	119.269	119.475	119.507
18H-10C-19C	122.616	122.341	122.198	122.018	121.990
10C-11C-12C	119.535	119.922	120.067	120.202	120.217
12C-11C-13N	117.117	116.658	116.475	116.277	116.252
11C-12C-14O	122.920	123.293	123.464	123.604	123.625
14O-12C-15O	122.581	122.139	121.877	121.561	121.505
12C-15O-21H	106.994	107.135	107.229	107.443	107.486

liquid sample analysis, a solution of 8HQC was prepared at 25 mg/mL and the pure solvent spectrum was recorded as reference before sample measurement. Due to the poor solubility of 8HQC in benzene and ether, experimental FT-IR spectra are only recorded in ethanol and water.

Geometry optimizations, harmonic frequencies, IR spectra in the gas phase and in solution phase were computed at B3LYP/6-311++G(d, p) for monomer forms and B3LYP/6-31G(d) level for dimer forms by using the Gaussian 09W suite of programs [11]. The solvent effects were evaluated by using the PCM. Geometries were fully optimized without symmetry constraints. The stationary structures were found by ascertaining that all the computed frequencies were real. Assignments for the fundamental vibrational modes were proposed according to their PED (potential energy distribution) values obtained by using the VEDA 4 program [12]. Frontier molecular orbitals properties, natural bond orbital (NBO) charges, and dipole moments were calculated. The aromaticity index NICS values were calculated by using the gauge independent atomic orbital (GIAO) method at B3LYP/6-311++G(d, p) level. The NICS probes (Bq) were placed at the geometric center of the benzene and pyrazine rings, and 1 Å above the ring center perpendicular to the ring plane.

Table 3. Scaled vibrational wavenumbers (frequency, cm^{-1}) of 8HQC in different media

Vacuum*		Benzene		Ether		Ethanol		Water		% PED*
frequency	I_{IR}	frequency	I_{IR}	frequency	I_{IR}	frequency	I_{IR}	frequency	I_{IR}	
59	2.14	58	2.77	60	3.27	64	3.91	64	4.06	71Γ(OCCC)
83	2.92	83	3.80	83	4.40	82	5.51	82	5.71	63Γ(NCCC)
154	9.83	163	12.55	165	14.45	162	17.15	160	17.65	47δ(NCC) + 15δ(CCC) + 13δ(OCC)
180	1.42	179	1.87	179	2.29	179	3.17	179	3.37	69 Γ(CCCC) + 15 Γ(OCCC)
202	1.39	202	1.49	201	1.50	201	1.45	200	1.43	51 Γ(CCCC) + 16 Γ(NCCC)
272	10.32	269	13.11	267	14.61	263	16.85	262	17.29	45 δ(OCC) + 18 δ(CCC)
297	3.99	297	4.79	297	5.39	297	6.42	297	6.64	52 Γ(CCCC) + 17Γ(NCCC) + 13Γ(OCCC)
331	0.30	332	0.31	333	0.35	333	0.50	333	0.54	33 ν(XX) + 16 δ(OXO)
428	6.81	429	10.84	429	13.98	430	19.43	430	20.41	24 Γ(NCCC) + 14Γ(CCCC) + 12Γ(HCCC) + 11Γ(HOCC)
465	21.27	465	28.55	465	33.52	463	40.72	462	42.04	54 δ(OCC)
491	23.65	480	70.43	474	88.98	466	118.41	465	124.36	39 Γ(HOCC) + 12Γ(NCCC)
498	28.70	495	2.98	495	1.43	495	0.66	495	0.59	43 Γ(HOCC) + 13Γ(NCCC)
508	0.72	508	0.95	508	1.14	508	1.55	508	1.64	28 δ(CCC) + 17 δ(OCC)
538	2.79	538	4.07	538	4.95	538	6.18	538	6.40	38 δ(CCC)
569	0.55	568	0.72	568	0.79	567	0.83	567	0.83	43 δ(CCC) + 17 δ(OCC) + 13 δ(NCC)
588	2.75	588	2.33	589	2.17	588	2.15	588	2.18	22 Γ(CCCC) + 21Γ(OCCC) + 13Γ(NCCC)
615	2.85	614	3.70	614	4.21	614	4.96	614	5.09	26 δ(CCC) + 26 δ(OCO)
638	117.87	641	101.06	643	84.10	644	84.12	644	87.80	57 Γ(HOCC)
647	20.40	651	53.25	654	82.44	658	105.97	658	107.57	31 Γ(HOCC) + 14 Γ(OCCC) + 14 Γ(OCOC)
729	20.26	729	28.88	729	35.08	728	44.57	728	46.34	32 δ(CCC) + 21 δ(OCO)
740	11.40	740	14.81	740	16.38	741	17.83	741	18.01	14 δ(NCC) + 12 δ(OCO) + 12 ν(CC)
762	43.57	765	53.60	766	60.81	766	71.65	766	73.50	34 Γ(CCCH) + 14 Γ(CCCC) + 10 Γ(NCCC)
769	0.26	772	0.03	773	0.06	773	0.92	773	1.39	34 Γ(CCCH) + 21 Γ(OCOC)
810	14.05	813	18.79	814	21.46	816	24.67	816	25.19	23 Γ(NCCC) + 11 Γ(CCCH) + 10 Γ(CCCC) + 10 Γ(NCCC)
870	39.28	870	45.47	870	49.71	868	56.47	868	57.80	71 Γ(CCCH)
883	12.87	883	17.69	883	20.97	882	25.85	882	26.76	53 δ(CCC)
901	0.49	904	0.46	905	0.44	905	0.41	905	0.41	77 Γ(CCCH)
925	1.57	925	1.98	925	2.24	924	2.60	924	2.66	19 δ(NCC) + 13 ν(CC) + 12 δ(CCC) + 10 ν(NC)
983	0.51	988	0.55	990	0.59	992	0.63	992	0.64	71 Γ(CCCH) + 16 Γ(CCCC)
1009	0.01	1011	0.10	1011	0.20	1011	0.37	1011	0.41	82 Γ(ccch) + 11 Γ(CCCC)
1066	1.84	1065	3.70	1065	5.39	1064	8.33	1064	8.91	43 ν(CC) + 19 δ(HCC)

Table 3. (Contd.)

Vacuum*		Benzene		Ether		Ethanol		Water		% PED*
frequency	I_{IR}	frequency	I_{IR}	frequency	I_{IR}	frequency	I_{IR}	frequency	I_{IR}	
1108	19.92	1107	35.24	1106	46.23	1104	63.11	1103	66.26	17 δ(CNC) + 13 ν(OC) + 11 δ(CCC) + 10 δ(HCC)
1128	68.31	1128	90.35	1128	104.62	1127	126.46	1127	130.59	51 ν(CC) + 13 ν(OC)
1155	4.47	1156	4.10	1155	4.36	1155	5.27	1154	5.52	58 δ(HCC) + 17 ν(CC)
1188	31.53	1187	48.89	1186	59.48	1183	73.45	1182	75.75	50 δ(HCC) + 11 δ(HOC)
1207	19.92	1203	22.31	1202	26.89	1199	42.34	1198	47.07	28 δ(HCC) + 14 δ(HOC)
1252	25.30	1250	93.40	1248	157.29	1245	255.87	1244	271.96	26 ν(CC) + 17 δ(HOC) + 10 δ(HCC)
1262	125.28	1259	119.84	1257	98.67	1255	60.88	1255	54.64	21 δ(HOC) + 21 δ(HCC) + 13 ν(OC)
1309	8.41	1308	18.66	1307	27.98	1306	45.09	1305	48.26	10 δ(HCC)
1344	80.75	1340	151.13	1338	199.62	1336	268.23	1336	279.42	27 ν(NC) + 13 δ(HOC) + 13 δ(HCC)
1379	312.50	1372	441.47	1369	495.12	1366	550.10	1365	558.19	23 δ(HOC) + 15 ν(CC) + 10 ν(NC)
1392	182.93	1390	154.17	1389	146.75	1388	133.88	1387	131.85	17 ν(NC) + 13 ν(CC) + 13 δ(HOC)
1414	16.84	1413	28.13	1412	35.84	1411	48.35	1411	50.91	17 δ(HOC) + 13 ν(NC) + 11 δ(NCC) + 10 δ(CC)
1464	3.57	1464	4.15	1463	4.75	1462	5.78	1462	6.00	47 δ(HCC)
1495	166.12	1492	212.97	1489	240.79	1487	277.37	1487	283.99	27 ν(NC) + 13 δ(HCC)
1540	66.23	1538	76.79	1536	81.95	1535	87.54	1535	88.12	22 δ(HCC)
1601	29.56	1600	33.37	1600	35.82	1599	39.51	1599	40.15	33 ν(CC) + 12 δ(CNC)
1626	2.59	1623	3.45	1622	3.97	1620	4.31	1620	4.41	33 ν(CC)
1663	20.76	1661	31.32	1660	39.14	1659	51.61	1659	54.15	53 ν(CC)
1822	403.31	1802	600.27	1791	727.68	1776	906.03	1773	937.55	85 ν(OC)
3167	1.15	3169	1.54	3170	1.75	3172	1.85	3172	1.85	89 ν(CH)
3169	4.86	3174	4.86	3177	4.72	3179	4.12	3180	3.97	88 ν(CH)
3182	13.38	3183	15.67	3184	17.42	3185	20.58	3185	21.24	99 ν(CH)
3195	3.66	3194	6.05	3194	8.17	3194	11.70	3194	12.37	96 ν(CH)
3212	2.19	3215	1.89	3216	1.65	3215	1.57	3215	1.60	97 ν(CH)
3658	148.21	3638	218.47	3629	259.50	3616	300.65	3614	305.57	98 ν(OH)
3730	55.77	3730	72.56	3729	83.83	3725	111.08	3721	117.79	99 ν(OH

* PED values given for calculation results in the gas phase [13].

RESULTS AND DISCUSSION

Implicit Consideration of Solvents

Energetics of 8HQC. Energies obtained from the DFT-PCM (B3LYP) optimizations of 8HQC are reported in Table 1 together with the theoretical gas phase data. Enthalpies, Gibbs free energies, and the relative Gibbs energy differences are also supplied [13].

As seen from Table 1, energy of 8HQC is gradually decreased while the dielectric constant of the media increased. Hence, the stability of the structure is increased due to the interactions between the solvent and the solute. In addition, the lowest energy value of 8HQC is obtained from the calculations carried out in aqueous solution.

Geometrical parameters. Optimized geometry of 8HQC in the gas phase is depicted in Fig. 1. Selected geometrical parameters are collected in Table 2, all bond lengths and angles are given in the Table S1, in

Table 4. NBO charges of 8HQC in different media.

Atom	Vacuum [13]	Benzene	Ether	Ethanol	Water
1C	–0.250	–0.252	–0.253	–0.255	–0.255
2C	0.336	0.334	0.333	0.332	0.332
3C	0.128	0.129	0.129	0.130	0.130
4C	–0.067	–0.066	–0.065	—-0.065	–0.064
5C	–0.215	–0.215	–0.215	–0.215	–0.215
6C	–0.160	–0.161	–0.161	–0.162	–0.163
7H	0.223	0.226	0.227	0.228	0.228
8H	0.210	0.215	0.218	0.221	0.221
9H	0.211	0.215	0.217	0.220	0.220
10C	–0.211	–0.210	–0.210	–0.209	–0.209
11C	0.118	0.114	0.112	0.110	0.109
12C	0.765	0.773	0.776	0.781	0.782
13N	–0.515	–0.511	–0.509	–0.504	–0.504
14O	–0.562	–0.586	–0.598	–0.614	–0.617
15O	–0.664	–0.672	–0.675	–0.679	–0.680
16O	–0.659	–0.667	–0.672	–0.677	–0.678
17H	0.485	0.490	0.493	0.497	0.497
18H	0.244	0.243	0.243	0.243	0.242
19C	–0.119	–0.116	–0.115	–0.113	–0.113
20H	0.214	0.220	0.223	0.227	0.228
21H	0.488	0.496	0.501	0.507	0.508

Supplement. Those parameters are presented following the order of dielectric constants of the media (vacuum $\varepsilon = 1$, benzene $\varepsilon = 2.2706$, ether $\varepsilon = 4.24$, ethanol $\varepsilon = 24.852$, water $\varepsilon = 78.3553$).

Introduction of solvents caused only small variations on the geometrical parameters of 8HQC. These variations are following the order of increasing dielectric constant of medium. The most significant variations are spotted at the carboxylic and hydroxylic sites. 12C–15O bond length is calculated as 1.343 Å in vacuum. This bond length is predicted as 1.342, 1.341, 1.340, and 1.339 Å in benzene, ether, ethanol, and water, respectively. Also, there is an intramolecular hydrogen bond between 13N···21H–15O which has a Y···H length of 2.060 Å in vacuum. This bond is predicted shorter when solvated with respect to the gas phase, though the shortest length is calculated in ether (2.047 Å) instead of water (2.049 Å). Another intramolecular hydrogen bond is proposed between 16O–17H···13N. In this bond, 16O–17H length is affected by the solvent at around 0.001 Å. On the other hand, 17H···13N distance is stretched significantly as much as 0.157 Å while passing from vacuum to solution. The calculated values for this length are 2.183, 2.187, 2.191, 2.198, and 2.199 Å, respectively.

Likewise the bond lengths, several bond angles are also changed. The 11C–10C–18H, 10C–11C–12C, and 11C–12C–14O angles become larger. On the other hand, 15O–12C–14O angle becomes tighter. Due to the stretching of 21H···13N bond, the 15O–12C–14O angle narrows. Hence, we may conclude that the hydrogen bonding between 15O–21H···13N become stronger when the system is solvated.

Vibrational modes. The optimized structure in this work gave all real frequencies at B3LYP/6-311++G(d, p) level. Those computed vibrational frequencies of 8HQC are scaled by 0.9982 [14] and given in Table 3. Theoretical vibrational spectra are shown in Fig. 2. We

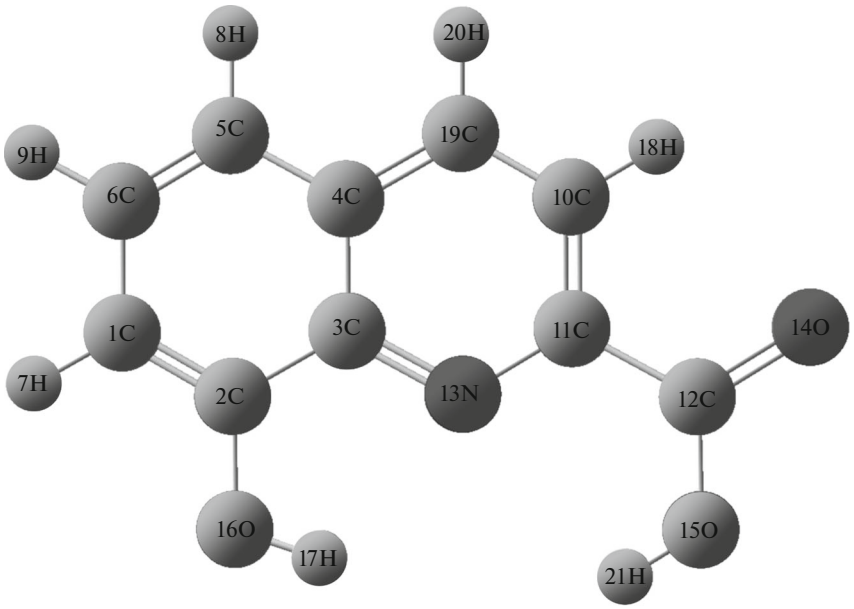

Fig. 1. Structure of 8HQC and atoms numbering in the gas phase.

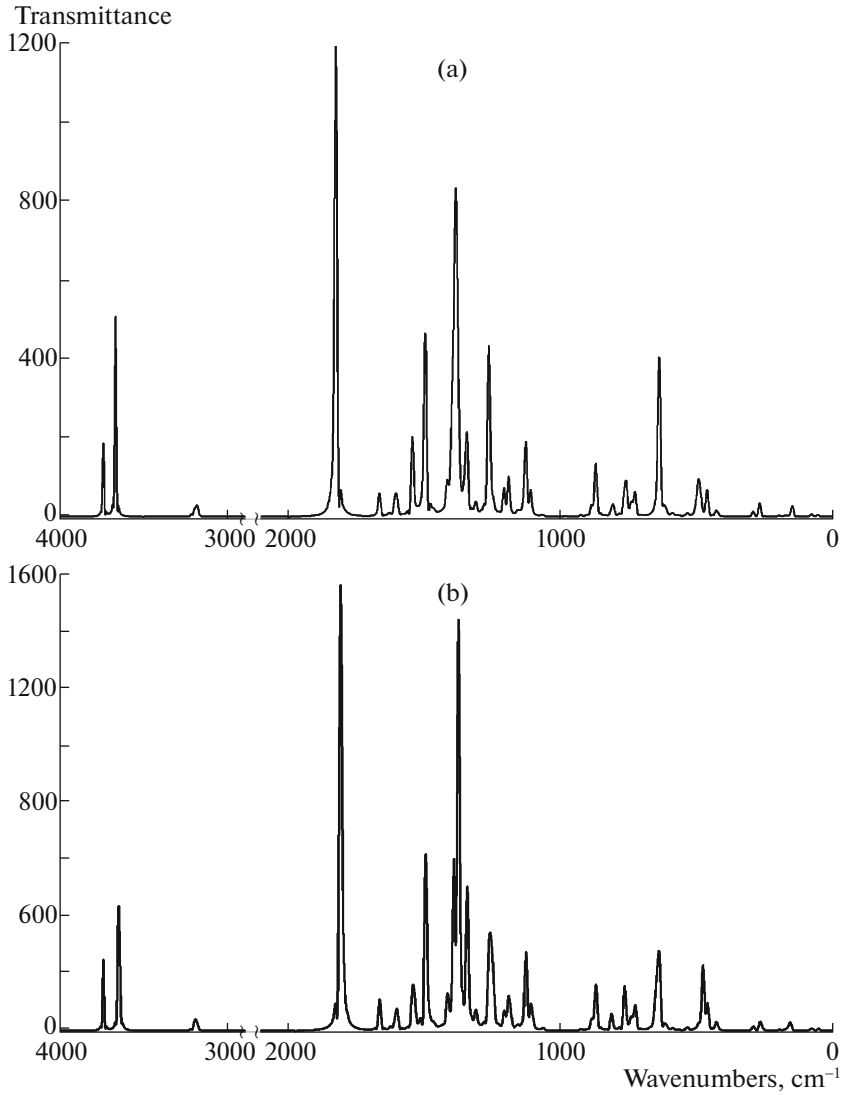

Fig. 2. Theoretical IR spectra for 8HQC in (a) vacuum, (b) benzene, (c) ether, (d) ethanol, (e) water.

will report only the most important vibrational frequencies hereafter.

Table 3 clearly shows that the vibrational frequencies of 8HQC are affected by the change of media. In the functional group region, 8HQC has five CH stretching modes computed at 3167, 3169, 3182, 3195, and 3212 cm^{-1} which are not significantly affected from the media. Among them, the mode at 3195 cm^{-1} is almost not affected by the dielectric media. The most affected CH stretching mode is the 3169 cm^{-1} which is shifted by 5, 7, 10, and 10 cm^{-1} in solution phase.

The characteristic carbonyl C=O stretching mode is calculated at 1822 cm^{-1}, and shifted to lower wavenumbers by 20, 31, 46, and 49 cm^{-1} when solvated following the order of dielectric constants. Another sig-

Table 5. Frontier molecular orbitals energies (Hartree) and ΔE_{L-H} gaps (eV) of 8HQC

Energy	Vacuum [13]	Benzene	Ether	Ethanol	Water
E_{HOMO}	−0.246	−0.242	−0.240	−0.238	−0.238
E_{LUMO}	−0.102	−0.099	−0.098	−0.097	−0.097
$\Delta E_{L\text{-}H}$	3.92	3.89	3.87	3.85	3.84

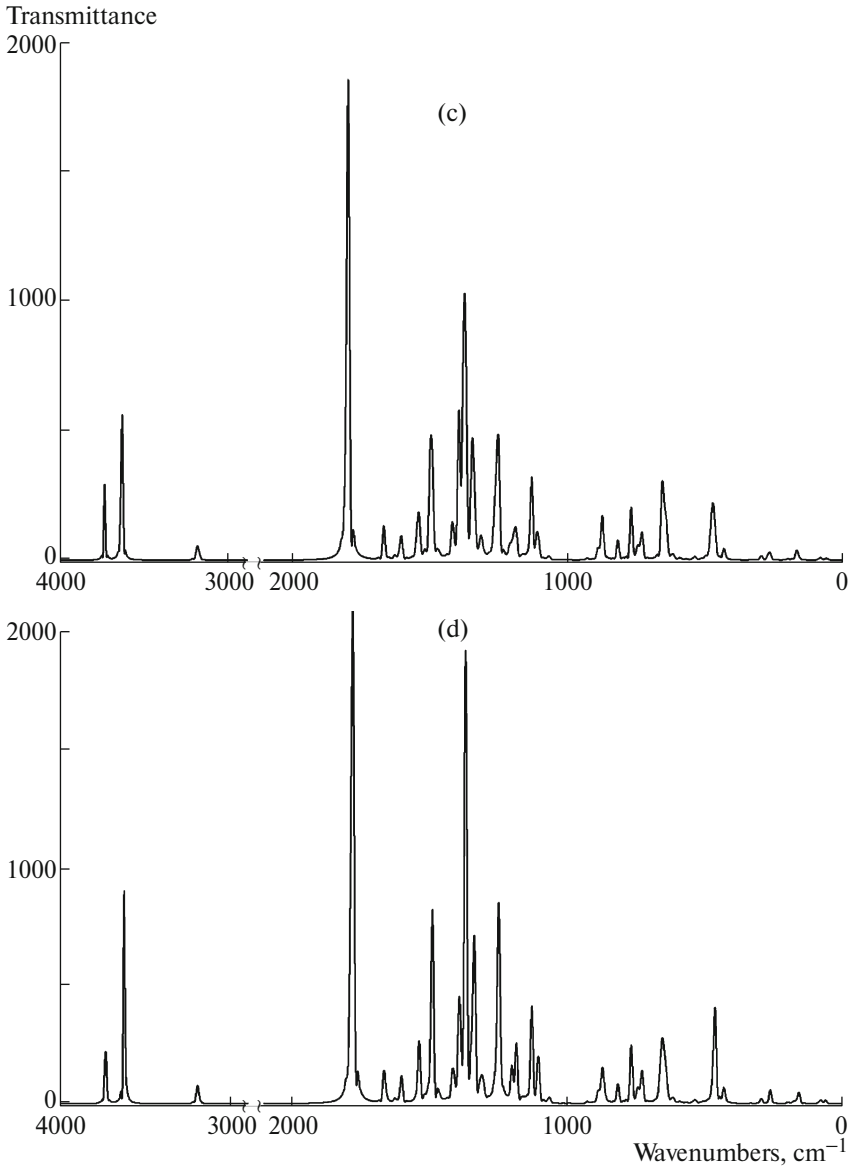

Fig. 2. (Contd.)

nificant change is occurred for the mode at 3658 cm^{-1}. This mode is OH stretching vibration which is related with the proposed hydrogen bonds between the pyridine nitrogen and hydroxyl and carboxyl groups. It is shifted by 20, 29, 42, and 44 cm^{-1}, respectively, in solution phase. The modes at 272, 491, 647, 1207,

Table 6. GIAO B3LYP/6-311++G(d, p) computed NICS values of benzene (bz) and pyridine (py) rings in the most stable 8HQC

Medium	$NICS(0)^{bz}$	$NICS(1)^{bz}$	$NICS(0)^{py}$	$NICS(1)^{py}$
Gas	−9.152	−10.501	−7.849	−10.620
Benzene	−9.090	−10.483	−7.871	−10.645
Ether	−9.047	−10.467	−7.888	−10.658
Ethanol	−8.970	−10.432	−7.916	−10.672
Water	−8.972	−10.433	−7.923	−10.676

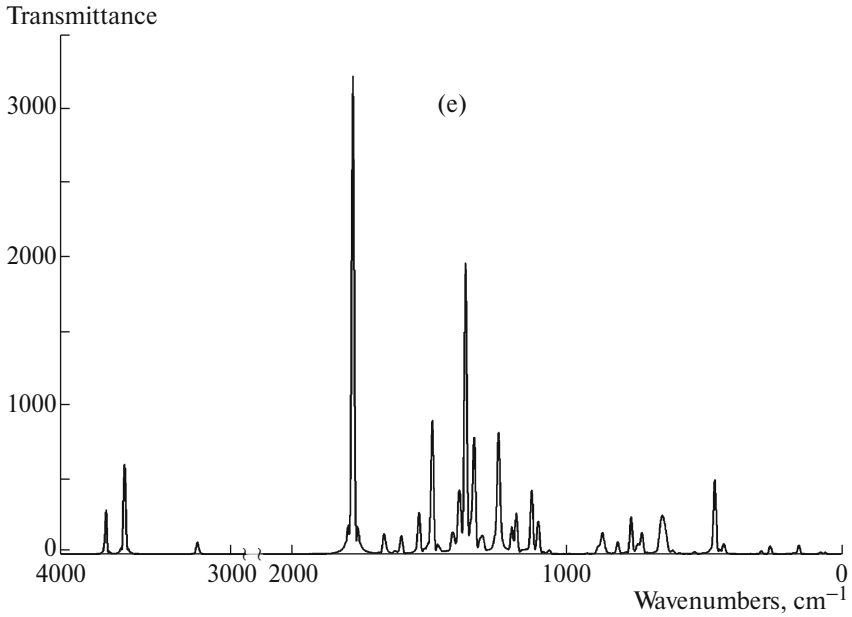

Fig. 2. (Contd.)

1252, and 1379 cm^{-1} have shown significant deviations. These modes are all related with the intramolecular hydrogen bonding, and they are shifted by up to 10, 26, 11, 9, 8, and 14 cm^{-1}, respectively, in aqueous solution. The most affected mode of those is 491 cm^{-1}. It is a mixed mode of OH torsion and puckering of the skeletal rings, and shifted by 10, 16, 24, and 26 cm^{-1} in solution phase in the order of dielectric constants.

According to our calculations while passing from gas phase to solution phase, most absorption peaks became stronger. Significant variations of IR intensities are determined in bands at 491, 647, 1252, 1822, and 3658 cm^{-1} has the largest changes in intensities (up to 534 km mol^{-1} in aqueous solution). The intensity of the OH mode at 3658 cm^{-1} is changed by 70, 111, 152, and 157 km mol^{-1}, respectively, in the solution phase. The C=O stretching band at 1822 cm^{-1} is the most affected band in terms of intensity. Its intensity is changed by 197, 324, 502, and 534 km mol^{-1}, respectively.

Dipole moments, NBO charges, and frontier molecular orbitals. Different compounds may display significant variations in their physical properties because of their different electronic structures. Such a physical property is the dipole moment. It is often used to discuss and rationalize the structure and reactivity of chemical systems [15]. Since the magnitude of the dipole moment is related with the stability in polar media, the prediction of dipole moments is an important issue [16]. The experimental dipole moment μ of 8HQC is not known. We have calculated dipole moment values of 8HQC as 5.179, 5.866, 6.198, 6.568, and 6.625 D, for which the order corresponds to the order of the dielectric constant values. It is concluded that due to larger dipole moment the 8HQC structure becomes more stable in solution.

The NBO charge distribution of 8HQC has been investigated in different media, and the results are given in Table 4. We have determined that the nitrogen of pyridine ring, oxygens of hydroxyl and carboxyl are rich in negative charges. This means that the atoms bonded to these atoms are electron donors. Our results indicate that the charge distribution on the pyridine ring is affected in quite small extent in overall. Hence, we have concluded that pyridine ring in the 8HQC structure is not much susceptible to the solvent effects. The negative charge on 13N decreased from −0.515 e in vacuum to −0.504 e in water. All of the oxygens in 8HQC gain negative charge on going from gas phase to aqueous solution. The charge on 14O increased from −0.562 e in vacuum up to −0.617 e in water, the charge on 15O increased from −0.664 e in vacuum up to −0.680 e in water, and the charge on 16O increased from −0.659 e in vacuum up to −0.678 e in water. These findings indicate that the charge distributions on oxygen atoms in 8HQC molecule are sensitive to dielectric medium.

In 1982, Fukui postulated that a good approximation for reactivity can be found by looking at the frontier orbitals [17]. The energy gap between these orbitals is considered as the measure of molecular chemical stability. We have investigated the frontier molecular orbitals properties to understand the reactivity of 8HQC in different media. The computed HOMO and LUMO energies in all media considered in this study are listed on Table 5. HOMO-LUMO contour plots are presented in Fig. S1, in Supplement.

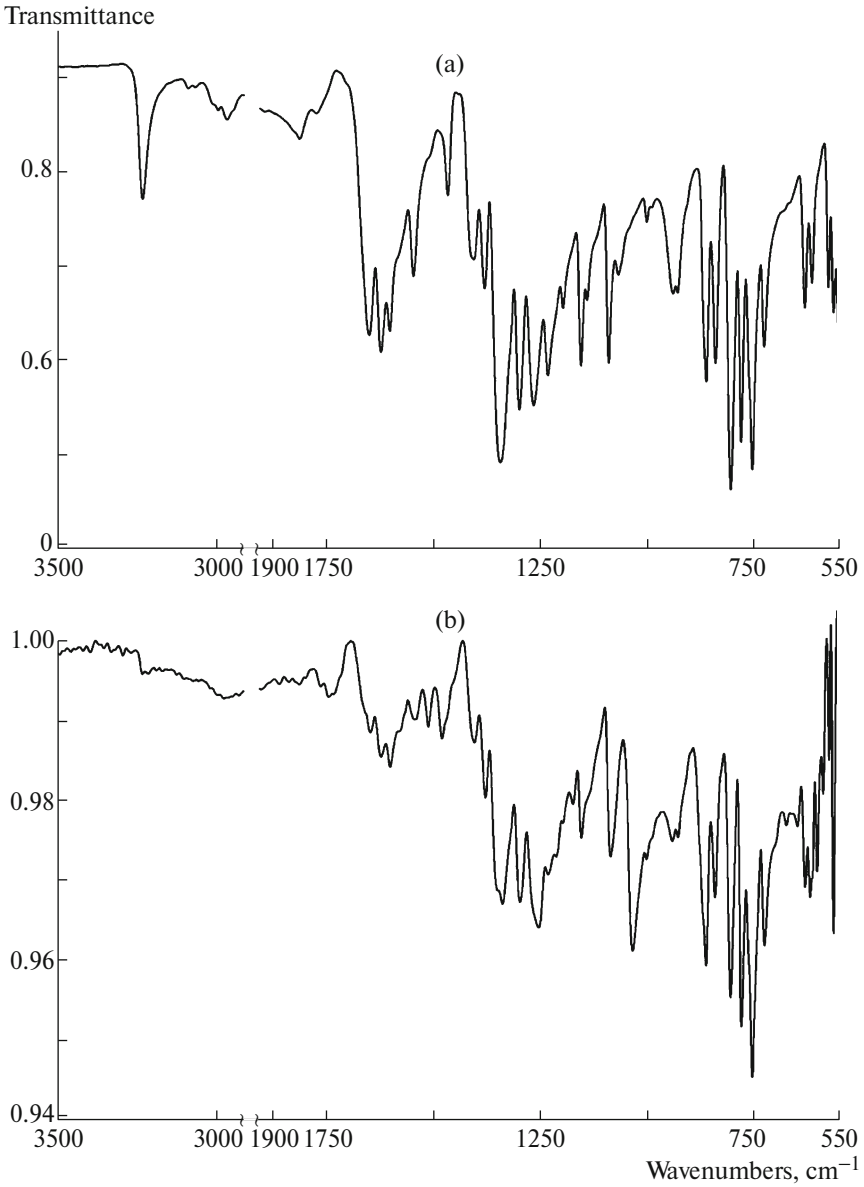

Fig. 3. ATR FT-IR spectra of 8HQC in (a) solid state [13], (b) ethanol, (c) water in the 3500–550 cm^{-1} spectral range.

Table 5 shows that both the LUMO and HOMO energies of 8HQC gradually decreasing with increasing dielectric constant of the medium. While passing from gas phase to solution phase, the energy gap ΔE_{L-H} is getting narrower. The magnitudes of the energy gap of 8HQC indicate that transfer of electrons from HOMO to LUMO is the easiest in aqueous solution. The increase in the net dipole moment of 8HQC in dielectric media, and possible formation of hydrogen bonds with solvent molecules are supposed to narrow the energy gap.

According to the HOMO-LUMO contour plots, the frontier electrons in HOMO orbital are localized over 11C–13O, 10C–19C, 1C–2C–3C, 4C–5C–6C, and 16O–17H. On the other hand, in LUMO orbital the frontier electrons are over 10C–12C, 2C–3C–4C–5C, 1C–6C, 16O, 15O, and 14O. These findings are true for all the media considered in this study. Hence, we may conclude that the frontier electron distribution over 8HQC atoms is not affected form the presence of a dielectric medium.

Aromaticity of 8HQC. Aromaticity is a chemical property associated with cyclic delocalization, and it is a useful tool to understand organic chemistry [18, 19]. There are several theoretical criteria of aromaticity which enable us to gather information on chemical properties of rings, such as structural stability and chemical reactivity. The magnetic criterion of aroma-

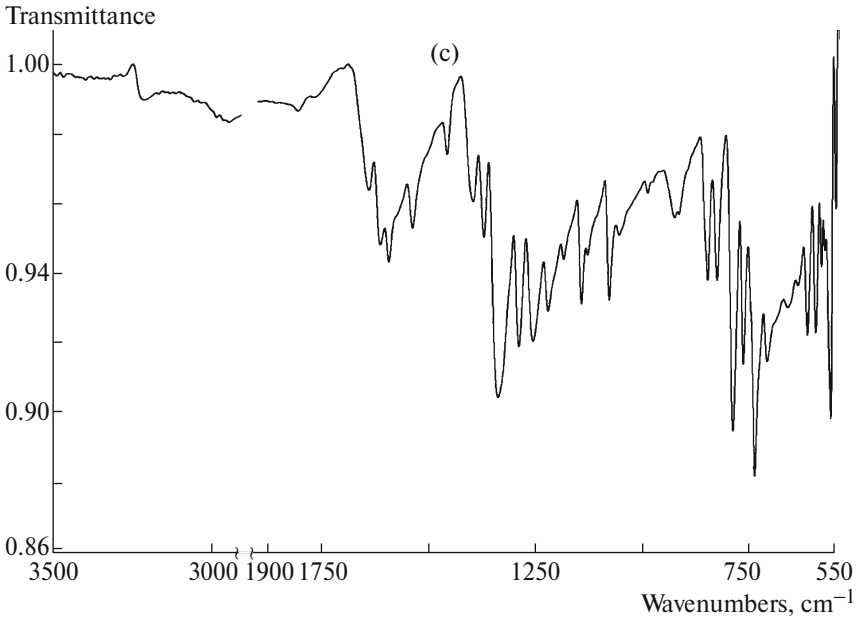

Fig. 3. (Contd.)

ticity is known as the nucleus-independent chemical shift (NICS) index which uses absolute magnetic shieldings computed at ring centers [18, 20]. By definition, rings with highly negative NICS values are classified as aromatic and a very small NICS value mean nonaromaticity [21]. The local effects of the σ-electron structure may significantly influence the NICS values, hence it is recommended to calculate the NICS at 1 Å above the ring. Table 6 shows the calculated NICS(0) and NICS(1) values of benzene and pyridine rings in 8HQC.

For points located at the center and at 1 Å above the ring centers of the benzene and pyridine rings, the data on Table 6 confirm that aromaticity of 8HQC changes with changing dielectric constant of the media. According to calculated NICS values, the benzene ring becomes less aromatic when 8HQC is solvated. Aromaticity of benzene ring decreases following the increasing order of dielectric constants. At the same time, aromaticity of pyridine ring increases in the same order. It has been seen that variations in aromaticity are small. Hence, the perturbation on the π-electron delocalization caused by the solution phase is weak.

Experimental Results and Explicit Consideration of Solvents in Calculations

There are three main approaches while investigating solvent effects theoretically: (i) implicit treatment (i.e., PCM method), (ii) explicit treatment (i.e., hydrogen bonded solute-solvent complexes in the gas phase), (iii) combination of the former two. We have chosen the latter approach in our study. Hydrogen bonded monomer and dimer forms of 8HQC are calculated, and then these results are used to interpret the experimental data.

Vibrational modes in ethanol. Experimental ATR FT-IR spectra of 8HQC are presented on Fig. 3. The experimental frequencies are gathered in Table 7, together with the PED values obtained from PCM B3LYP calculations carried out for the solution phase.

In the experimental solution phase spectrum there were several bands with various intensities which are not assignable to a monomer form. Therefore, we have additionally considered the most stable dimeric form of 8HQC [13] which stabilized by intermolecular hydrogen bonding. This dimer form's calculated frequencies can be seen in Table S2, in Supplement. Besides, ethanol is an H-donor solvent. We have observed that several bands have become broader when 8HQC solvated in ethanol. This could be explained by the possible formation of hydrogen bonded complexes. Hence we have computed a 1 : 1 8HQC-Ethanol complex at PCM B3LYP/6-311++G(*d*, *p*) level, and the complex' dimer form at the same level. Comparison of calculated data with the experimental data revealed that, in the solvated sample, 8HQC may be found both in its monomeric and dimeric forms. Considered structures are plotted in Fig. 4. For the interpretation of the experimental spectrum we have focused on changes observed between solid state and solution phase.

In solution phase spectrum, the bands observed at 560, 571, 627, 800, 837, 1345, 1474, 1539, 1642, 1758 cm^{-1} and most of the functional group region are

Table 7. Experimental and calculated vibrational frequencies, %PED values of 8HQC in ethanol solution together with the solid phase experimental data

Solid (exp.), cm^{-1} [13]	Ethanol soln. (exp.), cm^{-1}	$\|\Delta\|$, cm^{-1}	Source	Ethanol soln. (calc.) (I_{IR})	% PED
561 m	560 m	1	D	568 (6.13)	13Γ(HCOH) + 10δ(CCC) + 10Γ(CCOH) + 10Γ(OCOH)
573 m	571 m	2	D	573 (14.64)	20Γ(OCOH) + 10Γ(CCOH) + 10δ(CCC) + 10δ(CCO)
612 m	615 m	3		618 (6.86)	25 δ(CCC) + 24δ(OCO)
629 m	627 m	2	D	624 (21.61)	24δ(CCC) + 13δ(CCH) + 10ν(CC)
723 m	721 m	2		732 (38.33)	22δ(CCC)
751 vs	750 vs	1		749 (89.66)	15Γ(HOCC) + 12Γ(OHOH) + 10Γ(OHOC)
777 s	775 s	2		772 (87.36)	23Γ(HCCC) + 22Γ(OCOC) + 12Γ(OHOC)
801 vs	800 s	1	D	807 (73.79)	28Γ(OCOH) + 15Γ(OHOH)
837 m	837 m	0	D	834 (37.70)	32Γ(OCOH) + 16Γ(OHOH)
858 m	857 m	1		866 (61.04)	48Γ(HCCC) + 13Γ(OCOC) + 11Γ(NCCC)
925 m, 935 m sp	924 m, 936 m sp	1		925 (3.85)	18δ(NCC) + 12ν(CC) + 11δ(CCC)
986 w	986 w	0		987 (0.62)	79Γ(HCCC) + 15Γ(CCCC)
998 w	997 w	1		1006 (0.36)	83Γ(HCCC) + 10Γ(CCCC)
1064 m	1029 s	35		1033 (214.78)	57ν(CC) + 25ν(OC)
1087 m	1081 m	6		1070 (31.04)	36Γ(HCCO) + 16ν(OC)
1137 m	1134 sh	3		1127 (54.77)	46ν(OC) + 15δ(HOC) + 13ν(CC)
1151 m	1149 m	2		1150 (8.26)	57δ(HCC) + 16ν(CC)
1193 m	1191 m	2		1188 (42.68)	36δ(HCC) + 17δ(HOC)
1262 s	1248 s	14		1254 (193.22)	20δ(HCC) + 15ν(CC) + 11δ(HOC)
1296 s	1292 m	4		1296 (141.56)	15ν(OC) + 10δ(HOC) + 10δ(HCC)
1316 sh	1333 m	17		1329 (311.40)	21δ(HCC) + 17ν(OC) + 13ν(CC)
1340 vs	1345 m	5	D	1358 (134.34)	21δ(CCH) + 16δ(CCC) + 16ν(CC)
1377 m	1373 m	4		1383 (59.38)	21ν(NC) + 13δ(HOC) + 12ν(CC)
1400 m	1399 w	1		1402 (14.98)	69ν(HCH)
1462 m	1474 w	12	D	1473 (7.87)	27Γ(HCCH) + 19δ(HCH) + 13Γ(HCCO)
1507 sh	1506 w	1		1516 (5.59)	79δ(HCH)
1542 m	1539 w	3	D	1531 (1.33)	35δ(CCH) + 23ν(CC)
1598 m	1595 m	3		1598 (45.40)	33ν(CC) + 11ν(NC)
1620 m	1617 m	3		1621 (3.35)	33ν(CC)
1646 m	1642 w	4	D	1643 (0.01)	23ν(CC) + 20δ(CCH) + 11δ(CCC)
1770 w	1758 w	12	D	1691 (1744.86)	15ν(OC) + 13ν(CC) + 11δ(COH)
1808 w	1810 w	2		1751 (876.00)	84ν(OC)
3046 w	3044 w	2	D	3067 (2.44)	80ν(CH)
3070 w	3070 w	0	D	3075 (21.89)	92ν(CH)
3083 w	3089 w	6	D	3090 (38.50)	97ν(CH)
3131 w	3121 vw	10	D	3123 (5.23)	97ν(CH)
3150 w	3160 vw	10		3169 (3.18)	97ν(CH)
3271 m	3271 w	0	D	3596 (46.42)	97ν(OH)

ν: stretch, δ: bend, Γ: torsion, vw: very weak, w: weak, m: medium, sh: shoulder, s: strong, vs: very strong, sp: split, D: dimer form.

Table 8. Experimental and calculated vibrational frequencies, %PED values of 8HQC in aqueous solution together with the solid phase experimental data

Solid (exp.), cm^{-1} [13]	Aq. soln. (exp.), cm^{-1}	$\|\Delta\|$, cm^{-1}	Source	Aq. soln. (calc.) I_{IR}	% PED
561 m	560 m	1		560 (20.40)	21δ(CCC) + 11δ(CCO)
573 m	572 vs	1		586 (9.06)	21Γ(CCCC) + 19Γ(OCCC) + 11Γ(NCCC)
612 m	607 s	5		606 (47.30)	34δ(HOH) + 12δ(CCO)
629 m	627 s	1		624 (35.84)	31δ(CCC) + 19δ(OCO)
723 m	720 s	3		732 (70.83)	14ν(CC) + 11δ(CCC)
751 vs	749 vs	2		764 (247.23)	60Γ(HCCC)
777 s	775 s	2		772 (99.27)	48δ(OCO) + 10ν(OC)
801 vs	799 vs	2		794 (378.97)	18Γ(HOHO) + 12Γ(HOCC) + 11Γ(HCCC)
837 m	836 m	1		826 (2.95)	11Γ(CCCN) + 10Γ(CCCC) + 10Γ(OCOC)
858 m	857 m	1		865 (89.91)	59Γ(HCCC)
925 m, 935 m sp	924 m, 936 m sp	1		925 (3.69)	17δ(CCN)
998 w	997 w	1		1005 (1.52)	75Γ(HCCC)
1064 m	1064 m	0	M	1066 (12.36)	41ν(CC) + 18δ(HCC)
1087 m	1085 m	2		1070 (19.41)	42ν(CC) + 16δ(HCC)
1137 m	1136 m	1	M	1127 (46.98)	44ν(OC) + 16δ(HCC) + 12ν(CC)
1151 m	1150 m	1		1158 (9.18)	57δ(HCC)
1193 m	1191 m	2		1185 (132.46)	16δ(HCC) + 11ν(OC) + 10δ(HCN)
1262 s	1262 s	0		1261 (699.55)	12δ(HCC) + 11δ(HOC) + 10ν(OC)
1296 s	1295 s	1		1285 (1311.85)	20ν(OC) + 15δ(HOC)
1340 vs	1343 vs	3		1358 (260.71)	38ν(CC) + 12δ(HCC)
1377 m	1375 m	2		1380 (24.68)	12ν(NC) + 11δ(HOC) + 10ν(CC)
1400 m	1400 m	0		1403 (139.80)	34ν(NC) + 21ν(CC)
1462 m	1460 m	2		1457 (169.89)	54δ(HCC)
1507 sh	1503 sh	4		1496 (0.06)	15δ(OHO) + 12ν(OC)
1542 m	1541 m	1		1530 (205.00)	24δ(HCC) + 19ν(CC)
1598 m	1595 m	3		1584 (28.56)	38ν(CC)
1620 m	1615 m	5		1615 (56.78)	45δ(HOH) + 13Γ(HOHO)
1646 m	1641 m	5		1647 (260.04)	46ν(CC)
1770 w	1770 w	0		1661 (0.11)	45ν(OC) + 13δ(OHO)
1808 w	1808 w	0	M	1750 (901.00)	86ν(OC)
3046 w	3034 w	12		3169 (10.19)	97ν(CH)
3070 w	3066 w	4		3177 (33.44)	96ν(CH)
3083 w	3081 w	2		3182 (9.94)	96ν(CH)
3131 w	3125 w	6		3190 (14.63)	94ν(CH)
3150 w	3142 w	8		3370 (24.34)	99ν(OH)
3271 m	3258 w	13		3853 (58.52)	95ν(OH)

ν: stretch, δ: bend, Γ: torsion, vw: very weak, w: weak, m: medium, sh: shoulder, s: strong, vs: very strong, sp: split, M: monomer form.

originated from the 8HQC dimer. Many of these modes exhibit small shifts vary between 0–12 cm^{-1}.

In the 1800–1600 cm^{-1} region of the solid state spectrum, two carbonyl (OC) stretching modes have been observed at 1808 and 1770 cm^{-1} as weak bands. These bands are detected at 1810 (calc. 1751) and 1758 (calc. 1691) cm^{-1} on the spectrum recorded in ethanol. 2 and 12 cm^{-1} of shifts indicate that the carbonyl stretching mode is disturbed by the solvation. These shifts are due to the intermolecular hydrogen bonding between solute and solvent molecules. The band observed at 1262 cm^{-1} in solid state is shifted to 1248 (calc. 1254) cm^{-1}, and assigned to the mix of CC and CO vibrations. This mode is shifted by 14 cm^{-1} towards lower frequencies. A medium strong peak observed at 1064 cm^{-1} in solid state is shifted to 1029 (calc. 1033) cm^{-1} by 35 cm^{-1}, which is a mixed mode of CC and OC stretching vibrations. The mode at 1462 cm^{-1} in solid state was shifted by 12 cm^{-1} towards higher frequencies. It is identified at 1474 (calc. 1473) cm^{-1}, and assigned as the CH bending mostly contributed by ethanol.

Vibrational modes in water. The experimental frequencies of 8HQC in aqueous solution are gathered in Table 8, together with the PED values obtained from PCM B3LYP calculations carried out for the solution phase.

Likewise the solvation in ethanol, there were several bands which are not assignable to a monomer form. Also, several bands have become broader when 8HQC solvated in water. In order to interpret the experimental spectrum of aqueous solution we have carried out PCM B3LYP/6-311++G(d, p) level of calculations for 1 : 1 8HQC–water complex and the complex' dimer form. Considered structures are shown in Fig. 5. The dimer form's calculated frequencies can be seen in Table S3, in Supplement. Comparison of calculated data with the experimental data revealed that 8HQC is preferred to be in dimeric form. Hence, while interpreting the experimental results we have mostly used theoretical results of the dimer of 8HQC–water complex.

Table 9. Selected geometrical parameters of 8HQC from 1 : 1 complexes

Parameter	Ethanol	Water
2C-16C	1.349	1.350
11C-12C	1.504	1.504
12C-14O	1.214	1.214
12C-15O	1.334	1.335
11C-10C-18H	119.656	119.651
18H-10C-19C	121.954	121.946
10C-11C-12C	120.352	120.314
12C-11C-13N	116.275	116.278
11C-12C-14O	122.754	122.834
14O-12C-15O	121.073	121.022
12C-15O-21H	112.309	112.087

In solution phase spectrum, observed modes exhibit small shifts vary between 0–13 cm^{-1}, mostly 0–5 cm^{-1}. In the 1800–1600 cm^{-1} region of the aqueous solution spectrum, two carbonyl (OC) stretching modes are detected at the very same position as in the solid phase spectrum. They are spotted at 1808 (calc. 1661) and 1770 (calc. 1750) cm^{-1}. It seemed that the carbonyl stretching mode is not disturbed by the presence of aqueous medium. On the other hand, OH stretching bands are observed at 3258 (calc. 3853) cm^{-1} and 3142 (calc. 3370) cm^{-1}, exhibit some 13 and 8 cm^{-1} shifts. 3258 (calc. 3853) cm^{-1} is a weak peak in contrast to the medium strong peak observed in solid phase. The data presented on Table 8 shows a significant shift for a CH stretching band, namely 3034 cm^{-1}. This band is calculated at 3169 cm^{-1}, and it has been observed at 3046 cm^{-1} in solid phase spectrum. We may conclude that those shifts may arise due to the repulsive interactions between the ring hydrogens and water molecules. The rest of the shifts observed in aqueous solution IR spectrum of 8HQC is small and negligible.

Geometries of 8HQC in ethanol and in water. Selected geometrical parameters of 8HQC in both ethanol and in water are presented in Table 9. Table S4, in Supplement, tabulates the whole list. We have seen that including a solvent molecule explicitly in our calculations has not made significant differences when compared with the implicit PCM calculations.

Dipole moments, NBO charges, and frontier molecular orbitals. The dipole moment of 8HQC has been calculated as 5.1793 D in the gas phase. When solvents are implicitly considered, the dipole moment values of 8HQC are calculated as 6.5681 D in ethanol and 6.6246 D in water. When solvents are both implicitly and explicitly considered, obtained dipole moment values are 5.4785 D in ethanol and 5.5075 D in water for 1:1 complexes. Dipole moment values are predicted in larger quantities as expected. On the other hand, deviations from the gas phase result are small when compared with the implicit-only calculations.

Significant deviations in the NBO charges of 8HQC are spotted for the atoms 21H, 17H, 16O, 15O, 14O, 13N, and 12C. The list of NBO charges can be seen in Table S5, in Supplement. 21H, 17H, and 13N atoms lost negative charge due to hydrogen bonding interactions between the solute and the solvent. Negatively charged oxygen atoms are gained more negative charge, which refers to charge transfer from 12C to 14O and 15O.

The HOMO-LUMO contour maps of 1:1 complexes are shown in Figs. S2 and S3, in Supplement. We have identified no significant difference between

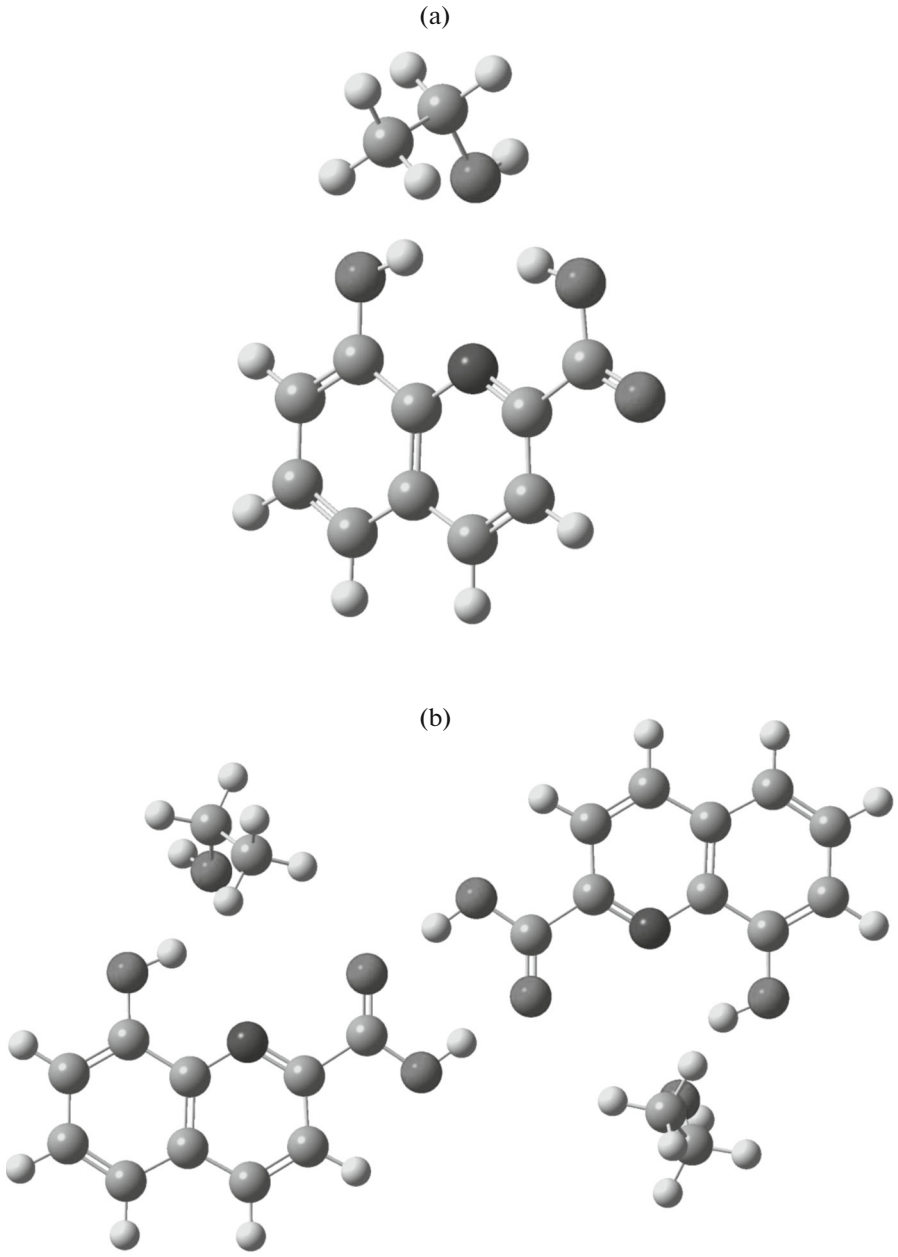

Fig. 4. Ethanol solution: (a) monomer, (b) dimer structures of 8HQC considered in this study.

those contour maps of the free ligand and 1:1 complexes. Hence, we may conclude that the frontier electrons distribution on 8HQC is not affected from the solvation. Besides, the HOMO-LUMO energy gaps are also calculated and found as 3.92, 3.87, and 3.87 eV in vacuum, ethanol, and water, respectively. We have concluded that there are no significant deviations occurred by the inclusion of explicit solvent molecules.

CONCLUSIONS

We have investigated the spectroscopic, structural, and electronic properties of 8HQC theoretically in benzene, ether, ethanol, and water. It has been seen that there is a relationship between the dielectricity of the media and the investigated properties of 8HQC. Total energy of 8HQC is gradually decreased while the dielectric constant of the media increased. Hence, the stability of the structure is increased. Introducing the solvation model caused only small variations on the geometrical parameters of 8HQC. The vibrational frequencies are affected by the change of medium. Stretching and bending vibrations C=O and O–H are significantly affected. Besides, we have seen that most absorption peaks became stronger in solution phase.

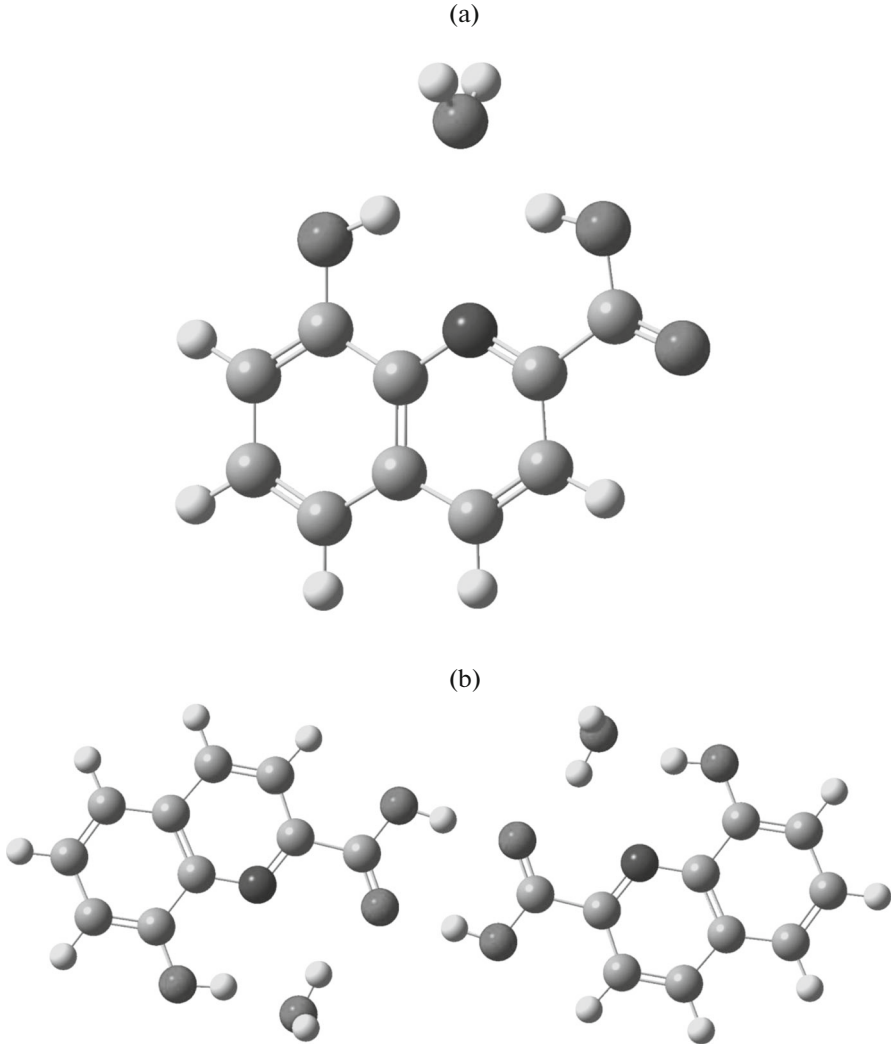

Fig. 5. Aqueous solution: (a) monomer, (b) dimer structures of 8HQC considered in this study.

The dipole moments are correlated with the dielectric constants of the media, and due to larger dipole moment the 8HQC structure becomes more stable in solution. The NBO charge distribution of 8HQC shows that the nitrogen of pyridine ring, oxygens of hydroxyl and carboxyl are rich in negative charges. The charge distribution on the pyridine ring is affected in quite small extent, though the charge distributions on oxygen atoms are found to be sensitive to dielectric medium. On the other hand, it has been seen that the frontier electron distribution over 8HQC atoms is not affected form the presence of a dielectric medium. Nucleus independent chemical shifts were calculated as aromaticity indices. Calculation results showed that the perturbation on the π-electron delocalization caused by the solution phase is weak. Also, we have found that NICS indices of aromaticity in 8HQC exhibit a logarithmic relation with dielectricity of the solvent.

Experimental FT-IR spectra in ethanol and in water are investigated. In the solution phase ATR FT-IR spectrum, several bands have become broader and several new bands observed. C=O and O–H frequencies are shifted. These variations can be explained by the formation of hydrogen-bonded solute-solvent complexes, increase in the net dipole of the solute, and the small changes occurred in the equilibrium geometry. In addition we have found that 8HQC can be found as both monomeric and dimeric forms in the ethanol solution, on the other hand it is mostly in dimeric form in aqueous solution.

ACKNOWLEDGMENTS

We gratefully acknowledge the support of this work by The Scientific and Technological Research Council of Turkey (TUBITAK) under grant number 111T595.

SUPPLEMENT

Table S1. Geometrical parameters (Å, degrees) of 8HQC

Parameter	Vacuum [13]	Benzene	Ether	Ethanol	Water
1C-2C	1.377	1.377	1.377	1.377	1.377
1C-6C	1.411	1.412	1.412	1.412	1.413
1C-7C	1.083	1.083	1.083	1.083	1.083
2C-3C	1.428	1.429	1.429	1.429	1.429
2C-16O	1.351	1.353	1.354	1.355	1.355
3C-4C	1.428	1.429	1.429	1.430	1.430
3C-13N	1.357	1.356	1.355	1.355	1.355
4C-5C	1.415	1.415	1.415	1.416	1.416
4C-19C	1.417	1.417	1.417	1.417	1.417
5C-6C	1.377	1.377	1.377	1.377	1.377
5C-8C	1.084	1.084	1.084	1.083	1.083
6C-9C	1.084	1.084	1.084	1.084	1.084
10C-11C	1.413	1.412	1.412	1.412	1.412
10C-18H	1.082	1.081	1.081	1.081	1.081
10C-19C	1.372	1.373	1.373	1.373	1.373
11C-12C	1.510	1.507	1.506	1.504	1.504
11C-13N	1.322	1.322	1.322	1.322	1.322
12C-14O	1.203	1.206	1.207	1.210	1.210
12C-15O	1.343	1.342	1.341	1.340	1.339
15O-21H	0.973	0.975	0.976	0.976	0.976
16O-17H	0.969	0.969	0.970	0.970	0.970
19C-20H	1.085	1.085	1.084	1.084	1.084
2C-1C-6C	120.097	120.096	120.106	120.132	120.136
2C-1C-7H	119.065	119.191	119.256	119.325	119.345
6C-1C-7H	120.838	120.714	120.638	120.543	120.519
1C-2C-3C	119.813	119.821	119.826	119.835	119.834
1C-2C-16O	120.457	120.474	120.453	120.383	120.376
3C-2C-16O	119.730	119.705	119.721	119.782	119.790
2C-3C-4C	119.506	119.511	119.493	119.452	119.446
2C-3C-13N	117.944	117.972	118.004	118.066	118.073
4C-3C-13N	122.550	122.518	122.503	122.483	122.481
3C-4C-5C	119.307	119.300	119.313	119.348	119.355
3C-4C-19C	116.715	116.756	116.781	116.825	116.833
5C-4C-19C	123.978	123.945	123.906	123.827	123.812
4C-5C-6C	119.616	119.602	119.595	119.588	119.585
4C-5C-8H	119.452	119.465	119.467	119.462	119.458
6C-5C-8H	120.932	120.932	120.938	120.951	120.956
1C-6C-5C	121.661	121.671	121.667	121.647	121.645
1C-6C-9H	118.610	118.578	118.564	118.565	118.560
5C-6C-9H	119.729	119.751	119.769	119.789	119.795
11C-10C-18H	118.783	119.105	119.269	119.475	119.507
11C-10C-19C	118.601	118.554	118.533	118.508	118.503
18H-10C-19C	122.616	122.341	122.198	122.018	121.990
10C-11C-12C	119.535	119.922	120.067	120.202	120.217
10C-11C-13N	123.349	123.420	123.458	123.522	123.531
12C-11C-13N	117.117	116.658	116.475	116.277	116.252
11C-12C-14O	122.920	123.293	123.464	123.604	123.625
11C-12C-15O	114.499	114.568	114.659	114.835	114.870
14O-12C-15O	122.581	122.139	121.877	121.561	121.505
3C-13N-11C	118.661	118.659	118.650	118.626	118.621
12C-15O-21H	106.994	107.135	107.229	107.443	107.486
2C-16O-17H	107.254	107.447	107.572	107.777	107.812
4C-19C-10C	120.125	120.093	120.075	120.037	120.031
4C-19C-20H	119.247	119.320	119.347	119.375	119.379
10C-19C-20H	120.629	120.587	120.579	120.588	120.590

Table S2. B3LYP/6-311++G(d, p) level computed vibrational data of 8HQC dimer in ethanol

Frequency, cm^{-1}	Frequency*, cm^{-1}	I_{IR}	Frequency, cm^{-1}	Frequency*, cm^{-1}	I_{IR}
13	13	0.22	1007	1005	1.55
14	14	1.09	1048	1046	211.84
19	19	0.49	1048	1046	107.10
25	25	2.51	1073	1071	32.02
29	29	8.48	1073	1071	1.93
33	33	1.54	1089	1087	76.37
43	43	1.23	1089	1087	30.92
46	46	1.21	1107	1105	28.07
49	49	0.74	1107	1105	61.42
51	51	4.67	1161	1159	9.06
61	61	2.55	1161	1159	0.00
67	67	0.06	1174	1172	7.34
72	72	0.28	1175	1172	9.76
85	85	3.15	1187	1185	94.73
89	89	0.12	1189	1186	0.03
92	92	0.61	1191	1189	168.48
107	107	0.82	1192	1190	0.09
109	109	0.32	1227	1224	482.37
117	117	14.33	1227	1225	15.16
125	124	0.04	1264	1262	7.88
150	150	21.72	1265	1262	670.75
164	164	0.02	1280	1278	13.40
173	173	7.06	1284	1282	1081.51
174	174	0.05	1300	1298	87.84
201	200	2.15	1300	1298	5.05
204	204	0.15	1312	1310	710.38
222	221	88.87	1313	1311	51.59
228	228	0.19	1317	1314	0.45
260	260	0.54	1318	1315	421.76
261	261	20.51	1360	1358	292.20
298	298	0.47	1360	1358	134.34
300	300	0.05	1383	1380	8.01
321	320	0.72	1383	1381	0.34
335	335	10.64	1399	1397	33.40
344	344	5.45	1400	1397	0.09
376	376	0.04	1405	1403	158.85
434	433	0.11	1407	1404	0.10
434	433	0.58	1450	1447	180.99
441	440	6.99	1455	1452	1.89
441	440	2.15	1455	1453	48.33
478	478	0.24	1463	1460	1.73
486	485	37.52	1464	1461	152.00
498	497	2.92	1475	1473	7.87
499	498	0.00	1475	1473	9.47

Table S2. (Contd.)

Frequency, cm^{-1}	Frequency*, cm^{-1}	I_{IR}	Frequency, cm^{-1}	Frequency*, cm^{-1}	I_{IR}
523	522	0.02	1476	1473	1.55
527	526	34.12	1487	1485	3.69
541	540	0.95	1487	1485	4.70
545	544	21.80	1495	1493	735.72
569	568	6.13	1497	1494	0.04
574	573	14.64	1519	1517	4.19
587	586	7.30	1519	1517	6.18
587	586	0.31	1534	1531	1.33
622	621	1.77	1534	1531	209.24
625	624	21.61	1586	1583	0.03
644	643	240.18	1587	1584	31.79
645	644	62.84	1622	1619	68.41
657	656	27.33	1622	1619	0.10
659	658	22.95	1646	1643	0.01
732	731	0.02	1648	1645	256.80
734	733	65.88	1666	1663	0.16
753	751	0.06	1694	1691	1744.86
767	766	31.99	3001	2996	90.44
767	766	148.76	3001	2996	98.62
774	773	95.00	3030	3024	33.22
779	778	7.95	3030	3024	21.34
780	778	0.60	3035	3030	52.54
808	807	73.79	3035	3030	52.99
809	807	224.00	3097	3092	56.36
818	816	18.70	3097	3092	61.37
818	816	0.60	3098	3093	41.66
835	834	37.70	3098	3093	53.85
836	834	51.36	3105	3100	0.03
851	849	0.06	3167	3162	7676.23
868	866	75.96	3173	3168	14.94
869	867	0.79	3173	3168	34.50
882	881	0.06	3181	3176	0.14
883	882	65.66	3182	3176	75.04
889	888	44.11	3187	3181	4.89
889	888	40.34	3187	3181	35.43
902	900	12.39	3196	3190	0.62
902	900	2.35	3196	3190	8.85
924	922	333.62	3224	3218	3.72
926	924	0.06	3224	3218	0.16
927	925	4.01	3305	3299	1470.22
991	989	0.00	3307	3301	1492.35
991	989	1.05	3641	3635	1403.96
1007	1005	0.00	3642	3635	71.68

* 0.9982 was used as the scaling factor.

Table S3. B3LYP/6-311++G(d, p) level computed vibrational data of 8HQC dimer in water

Frequency, cm^{-1}	Frequency*, cm^{-1}	I_{IR}	Frequency, cm^{-1}	Frequency*, cm^{-1}	I_{IR}
11	11	0.66	901	900	11.66
14	14	2.81	901	900	0.78
31	30	6.44	916	915	355.24
31	31	0.97	926	924	0.00
41	41	14.50	926	925	3.69
50	50	2.80	992	990	0.17
61	61	0.01	992	990	0.81
63	63	1.98	1007	1005	0.01
86	86	0.04	1007	1005	1.53
92	92	4.24	1071	1070	19.41
94	94	0.03	1072	1070	0.16
105	105	0.81	1106	1104	99.04
143	143	37.60	1106	1104	0.15
146	146	0.65	1161	1158	9.18
164	163	35.69	1161	1159	0.01
171	170	0.00	1187	1185	132.46
173	173	0.64	1189	1187	0.01
175	174	18.36	1190	1187	180.36
201	201	7.34	1190	1188	0.00
203	203	3.28	1225	1222	619.55
210	209	5.17	1225	1223	0.55
218	218	11.19	1262	1260	0.01
234	233	81.48	1263	1261	699.55
235	235	278.92	1285	1282	0.31
298	298	0.64	1287	1285	1311.84
300	299	0.14	1316	1314	31.42
304	304	1.84	1316	1314	518.30
322	322	56.02	1360	1358	260.71
338	337	15.24	1360	1358	143.02
374	373	4.11	1383	1380	24.69
393	392	71.02	1383	1381	0.24
393	393	114.65	1405	1403	139.80
434	433	1.53	1407	1405	0.10
434	434	0.35	1448	1445	193.85
476	475	0.85	1459	1457	0.09

Table S3. (Contd.)

Frequency, cm^{-1}	Frequency*, cm^{-1}	I_{IR}	Frequency, cm^{-1}	Frequency*, cm^{-1}	I_{IR}
484	483	44.51	1460	1457	169.89
498	497	3.11	1478	1475	0.01
499	499	0.01	1495	1493	717.33
522	521	0.78	1498	1496	0.00
527	526	27.23	1533	1530	0.71
539	538	7.86	1533	1530	205.00
542	541	34.60	1586	1583	0.82
561	560	20.40	1586	1584	28.56
566	565	0.76	1618	1615	98.71
587	586	9.06	1618	1615	56.78
587	586	2.33	1622	1619	13.73
607	606	47.30	1622	1619	185.41
609	608	287.15	1646	1644	0.29
624	623	3.09	1649	1647	260.04
626	624	35.84	1664	1661	0.12
657	656	12.85	1691	1688	1726.77
658	657	0.66	3104	3099	0.12
732	731	0.01	3160	3154	7760.00
734	732	70.83	3175	3169	10.19
753	752	0.05	3175	3169	15.78
766	764	247.23	3182	3177	0.00
766	764	24.80	3183	3177	33.44
774	772	99.27	3188	3182	9.94
779	777	0.02	3188	3182	28.96
779	777	0.94	3196	3190	0.67
795	794	34.66	3196	3190	14.62
796	794	378.97	3224	3218	3.23
828	826	2.95	3224	3218	0.25
828	827	1.26	3376	3370	24.34
865	863	0.07	3376	3370	2336.42
867	865	89.91	3623	3617	916.02
874	873	0.15	3624	3617	300.48
883	881	0.00	3860	3853	219.75
883	882	64.09	3860	3853	58.52

* 0.9982 was used as the scaling factor.

Table S4. Geometrical parameters (Å, degrees) taken from 1:1 8HQC:solvent complexes

Parameter	Ethanol	Water	Parameter	Ethanol	Water
1C-2C	1.380	1.380	2C-3C-4C	119.708	119.663
1C-6C	1.412	1.412	2C-3C-13N	117.890	117.922
1C-7C	1.083	1.083	4C-3C-13N	122.402	122.415
2C-3C	1.431	1.431	3C-4C-5C	119.455	119.468
2C-16C	1.349	1.350	3C-4C-19C	116.680	116.707
3C-4C	1.431	1.431	5C-4C-19C	123.866	123.825
3C-13N	1.352	1.352	4C-5C-6C	119.410	119.424
4C-5C	1.415	1.415	4C-5C-8H	119.557	119.505
4C-19C	1.418	1.418	6C-5C-8H	121.032	121.071
5C-6C	1.378	1.378	1C-6C-5C	121.697	121.678
5C-8H	1.084	1.084	1C-6C-9H	118.555	118.557
6C-9H	1.084	1.084	5C-6C-9H	119.747	119.765
10C-11C	1.414	1.414	11C-10C-18H	119.656	119.651
10C-18H	1.081	1.081	11C-10C-19C	118.390	118.403
10C-19C	1.373	1.373	18H-10C-19C	121.954	121.946
11C-12C	1.504	1.504	10C-11C-12C	120.352	120.314
11C-13N	1.318	1.318	10C-11C-13N	123.373	123.409
12C-14O	1.214	1.214	12C-11C-13N	116.275	116.278
12C-15O	1.334	1.335	11C-12C-14O	122.754	122.834
15O-21H	0.986	0.984	11C-12C-15O	116.173	116.144
16O-17H	0.981	0.979	14O-12C-15O	121.073	121.022
19C-20H	1.084	1.084	3C-13N-11C	119.013	118.952
2C-1C-6C	120.463	120.453	12C-15O-21H	112.309	112.087
2C-1C-7H	119.127	119.147	2C-16O-17H	111.810	111.594
6C-1C-7H	120.410	120.400	4C-19C-10C	120.142	120.114
1C-2C-3C	119.267	119.315	4C-19C-20H	119.266	119.264
1C-2C-16O	119.921	119.925	10C-19C-20H	120.592	120.622
3C-2C-16O	120.812	120.759			

Table S5. NBO charges of 1:1 8HQC:solvent complexes

Atom	Vacuum	Ethanol	Water	Atom	Vacuum	Ethanol	Water
1C	−0.250	−0.246	−0.246	12C	0.765	0.782	0.783
2C	0.336	0.334	0.333	13N	−0.515	−0.477	−0.479
3C	0.128	0.123	0.124	14O	−0.562	−0.630	−0.632
4C	−0.067	−0.066	−0.066	15O	−0.664	−0.705	−0.704
5C	−0.215	−0.222	−0.221	16O	−0.659	−0.705	−0.705
6C	−0.160	−0.175	−0.175	17H	0.485	0.520	0.522
7H	0.223	0.223	0.224	18H	0.244	0.239	0.240
8H	0.210	0.218	0.219	19C	−0.119	−0.123	−0.122
9H	0.211	0.218	0.218	20H	0.214	0.224	0.225
10C	−0.211	−0.211	−0.212	21H	0.488	0.529	0.532
11C	0.118	0.105	0.105				

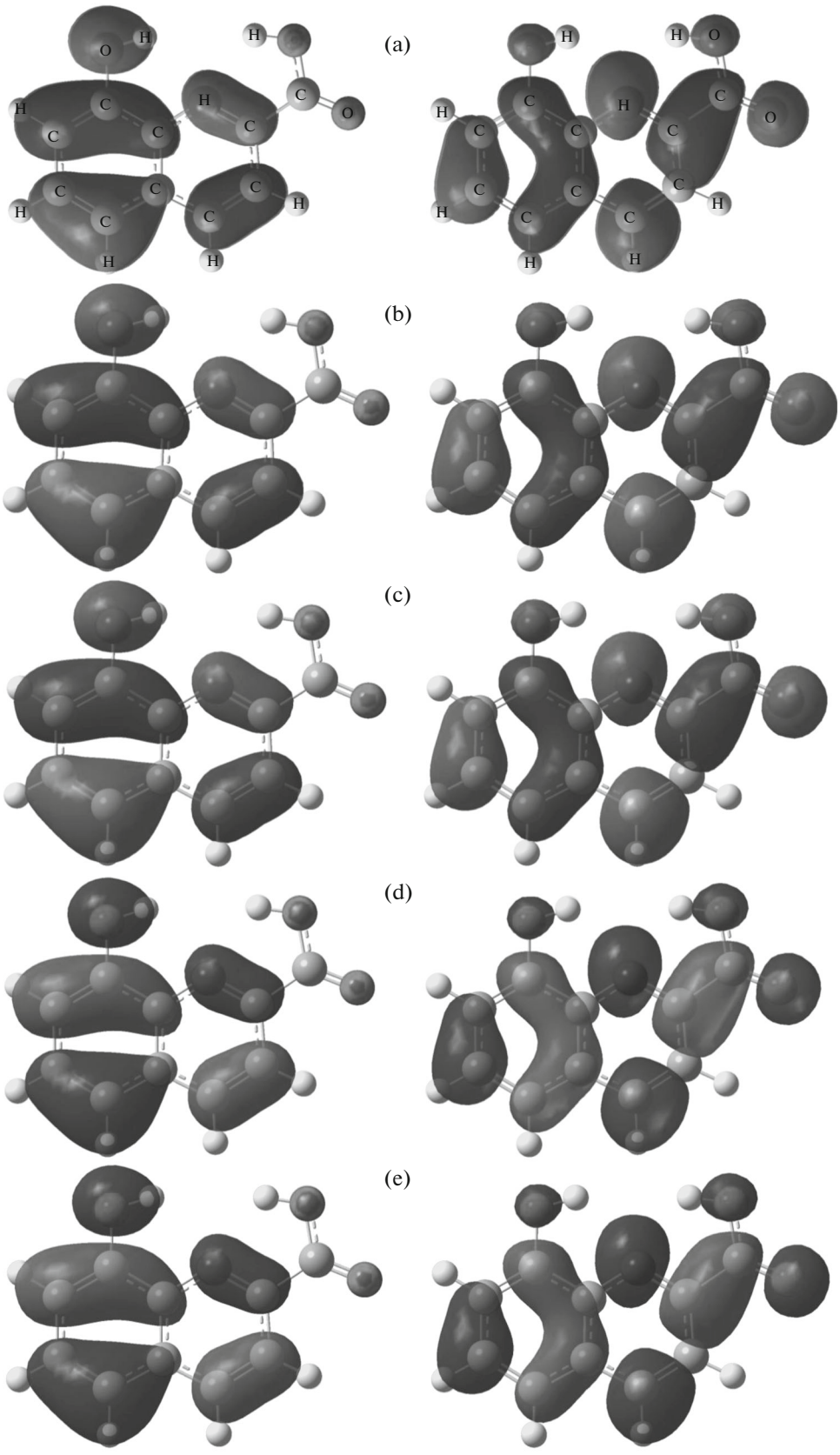

Fig. S1. HOMO (left-hand side) and LUMO (right-hand side) contour maps of 8HQC in different media: (a) vacuo [21], (b) benzene, (c) ether, (d) ethanol, (e) water.

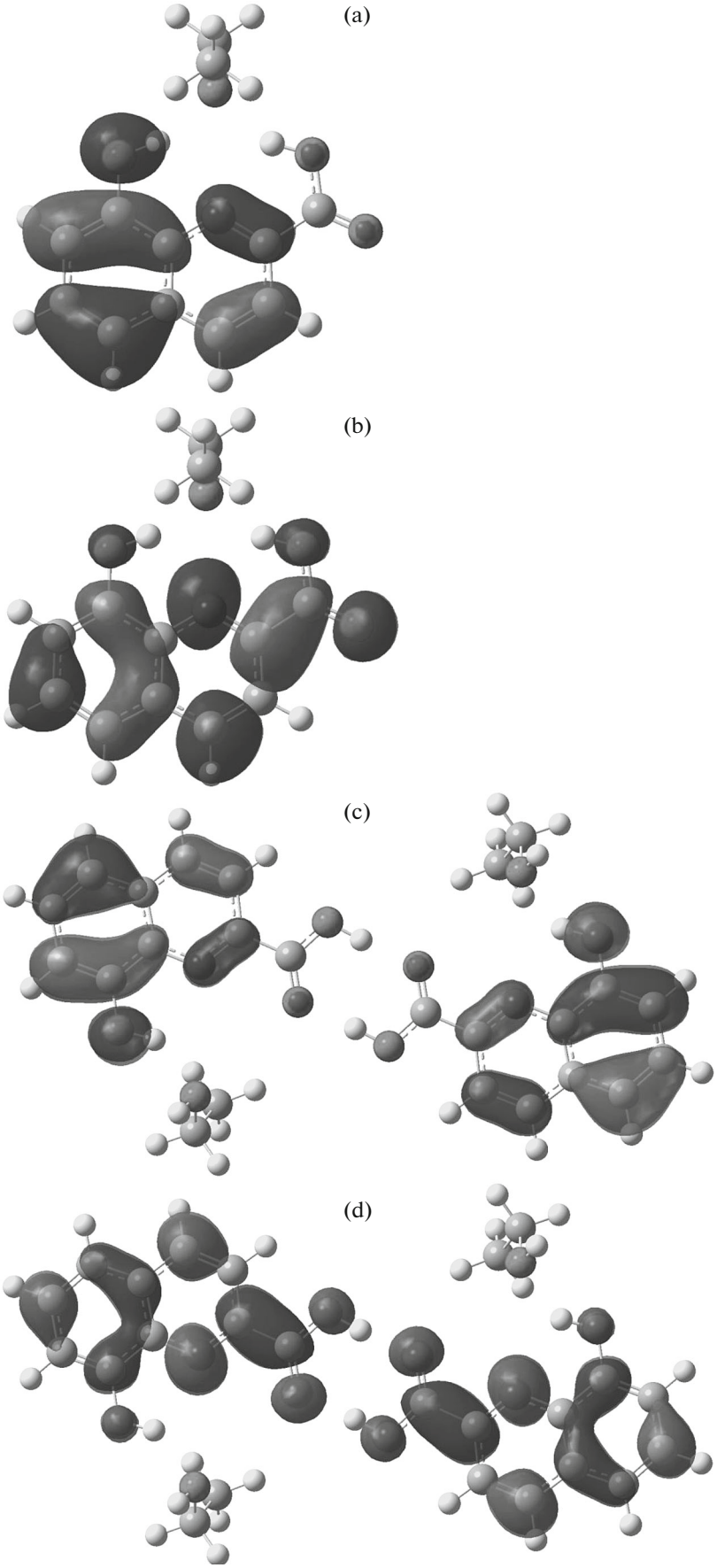

Fig. S2. In ethanol: (a) HOMO, (b) LUMO of 1:1 complex; (c) HOMO, (d) LUMO of dimer structure.

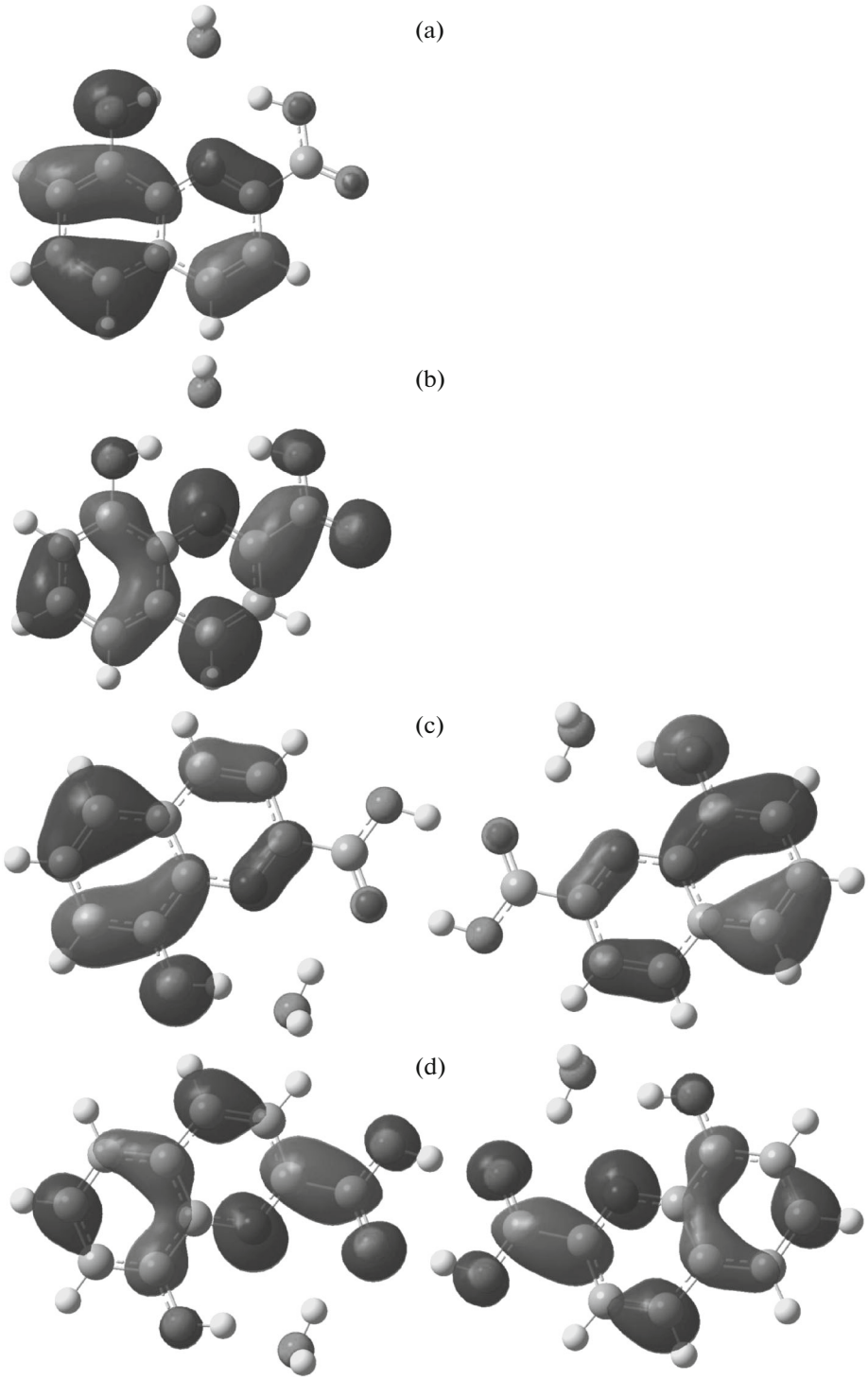

Fig. S3. In water: (a) HOMO, (b) LUMO of 1:1 complex; (c) HOMO, (d) LUMO of dimer structure.

REFERENCES

1. S. Chowdhury, F. Himo, N. Russo, and E. Sicilia, J. Amer. Chem. Soc. **132**, 4178 (2010).
2. C. Wang, Z. Y. Fang, H. Liu, and S. Xu, Int. J. Phys. Sci. **3**, 250 (2008).
3. S. Xu, C. Wang, G. Sha, J. Xie, and Z. Yang, J. Mol. Struct. Theochem **459**, 163 (1999).
4. M. A. Halim, D. M. Shaw, and R. A. Poirier, J. Mol. Struct. Theochem **960**, 63 (2010).
5. L. Rivail and D. Rinaldi, Theor. Chim. Acta **32**, 57 (1973).

6. S. Miertus, E. Scrocco, and J. Tomasi, Chem. Phys. **55**, 117 (1981).
7. R. J. Hall, M. M. Davidson, N. A. Burton, and I. H. Hillier, J. Phys. Chem. **99**, 921 (1995).
8. H. Oda, J. Soc. Dyers Colourists **114**, 363 (1998).
9. H. Oda, Dyes Pigments **37**, 165 (1998).
10. A. N. Pearce, W. N. Chia, M. V. Berridge, G. R. Clark, J. L. Harper, L. Larsen, E. W. Maas, M. J. Page, N. B. Perry, V. L. Webb, and B. R. Copp, J. Natur. Prod. **70**, 936 (2007).
11. M. J. Frisch, G. W. Trucks, H. B. Schlegel, G. E. Scuseria, M. A. Robb, J. R. Cheeseman, G. Scalmani, V. Barone, B. Mennucci, G. A. Petersson, H. Nakatsuji, M. Caricato, X. Li, H. P. Hratchian, A. F. Izmaylov, J. Bloino, G. Zheng, J. L. Sonnenberg, M. Hada, M. Ehara, K. Toyota, R. Fukuda, J. Hasegawa, M. Ishida, T. Nakajima, Y. Honda, O. Kitao, H. Nakai, T. Vreven, J. A. Montgomery, Jr., J. E. Peralta, F. Ogliaro, M. Bearpark, J. J. Heyd, E. Brothers, K. N. Kudin, V. N. Staroverov, R. Kobayashi, J. Normand, K. Raghavachari, A. Rendell, J. C. Burant, S. S. Iyengar, J. Tomasi, M. Cossi, N. Rega, J. M. Millam, M. Klene, J. E. Knox, J. B. Cross, V. Bakken, C. Adamo, J. Jaramillo, R. Gomperts, R.E. Stratmann, O. Yazyev, A. J. Austin, R. Cammi, C. Pomelli, J. W. Ochterski, R. L. Martin, K. Morokuma, V. G. Zakrzewski, G. A. Voth, P. Salvador, J. J. Dannenberg, S. Dapprich, A. D. Daniels, Ö. Farkas, J. B. Foresman, J. V. Ortiz, J. Cioslowski, and D. J. Fox, Gaussian 09, Revision **C**.1, 2009.
12. M. H. Jamroz, Vibrational Energy Distribution Analysis VEDA 4, 2004.
13. S. Badoğlu and Ş. Yurdakul, Opt. Spectrosc. **116**, 196 (2014).
14. H. Watanabe, N. Hayazawa, Y. Inouye, and S. Kawata, J. Phys. Chem. B **109**, 5012 (2005).
15. A. Chatterjee, T. Balaji, H. Matsunaga, and F. Mizukami, J. Mol. Graph. Modell. **25**, 208 (2006).
16. M. A. Palafox, G. Tardajos, A. Guerrero-Martinez, V. K. Rastogi, D. Mishra, S. P. Ojha, and W. Kiefer, Chem. Phys. **340**, 17 (2007).
17. K. Fukui, Science **218**, 747 (1982).
18. P. V. R. Schleyer and H. Jiao, Pure Appl. Chem. **68**, 209 (1996).
19. T. M. Krygowski, M. Cyrański, A. Ciesielski, B. Świrska, and P. Leszczynski, J. Chem. Inf. Comp. Sci. **36**, 1135 (1996).
20. P. V. R. Schleyer, C. Maerker, A. Dransfeld, H. Jiao, and N. J. R. van Eikema Hommes, J. Amer. Chem. Soc. **118**, 6317 (1996).
21. S. Badoğlu and Ş. Yurdakul, Struct. Chem. **21**, 1103 (2010).